

ThermoMaze: A behavioral paradigm for readout of immobility-related brain events

Mihály Vöröslakos^{*1}, Yunchang Zhang^{*1,3}, Kathryn McClain¹, Roman Huszár¹, Aryeh Rothstein¹, György Buzsáki^{†1,2}

^{*}These authors contributed equally to this work.

¹Neuroscience Institute and ²Department of Neurology, School of Medicine, New York University, New York, NY 10016, USA

³Princeton Neuroscience Institute, Princeton University, Princeton, NJ 08544, USA

[†]Correspondence: Gyorgy.Buzsaki@nyulangone.org

Abstract

Brain states fluctuate between exploratory and consummatory phases of behavior. These state changes affect both internal computation and the organism's responses to sensory inputs. Understanding neuronal mechanisms supporting exploratory and consummatory states and their switching requires experimental control of behavioral shifts and collecting sufficient amounts of brain data. To achieve this goal, we developed the ThermoMaze, which exploits the animal's natural warmth-seeking homeostatic behavior. By decreasing the floor temperature and selectively heating unmarked areas, mice avoid the aversive state by exploring the maze and finding the warm spot. In its design, the ThermoMaze is analogous to the widely used water maze but without the inconvenience of a wet environment and, therefore, allows the collection of physiological data in many trials. We combined the ThermoMaze with electrophysiology recording, and report that spiking activity of hippocampal CA1 neurons during sharp-wave ripple events encode the position of the animal. Thus, place-specific firing is not confined to locomotion and associated theta oscillations but persist during waking immobility and sleep at the same location. The ThermoMaze will allow for detailed studies of brain correlates of immobility, preparatory-consummatory transitions and open new options for studying behavior-mediated temperature homeostasis.

Introduction

All behaviors can be considered as parts of a sequence of action-rest transition¹. Brain states in vertebrates fall into dichotomous categories, and correspond roughly to what early behavioral research referred to as “preparatory” (or “exploratory”) and “consummatory” (or “terminal”) classes². In mammals, these two fundamental brain states can be readily identified by basic electrophysiological monitoring of various brain structures³. They are also referred to as voluntary and non-voluntary or conscious and non-conscious brain states³. Switching between these states is correlated with high and low release of subcortical neuromodulators⁴⁻⁹. Consummatory/terminal behaviors include feeding and drinking, resting and its extreme form, non-rapid eye movement (NREM) sleep, while preparatory/exploratory behaviors include locomotion and other movements that are a result of a general tendency to sample environmental stimulus. Preparatory and consummatory behaviors in the hippocampus are associated with theta oscillations and sharp wave ripples (SPW-Rs), respectively¹⁰.

Deciphering the physiological underpinnings of these categories and revealing the significance of brain state transitions for cognition requires sufficient sampling of the relevant brain states. This is usually achieved by extended repeated recordings or, when possible, recording large numbers of neurons simultaneously. Prolongation of exploratory behavior can be readily achieved by placing the animal in novel environments, by food or water deprivation or by introducing delays in choice behavior tasks^{11,12}. Recently, the honeycomb maze paradigm was introduced to extend the observation periods of exploratory deliberation¹³.

In contrast, the experimental control of consummatory behavioral classes is more difficult. Sleep provides an opportunity for long recordings. Comparison of sleep before and after learning is a standard paradigm to examine experience-induced brain plasticity^{14,15}. Consummatory brain states associated with eating, drinking, and sex change rapidly with satiety and require prolonged periods of deprivation¹⁶⁻¹⁹. Controlling periods of awake immobility is most difficult²⁰⁻²², mainly because forced immobilization of the animal is stressful²³ and is accompanied by altered physiological states²⁴.

Here we introduce the ThermoMaze, a behavioral paradigm that allows for the collection of large amounts of physiological data while the animal rests at distinct experimenter-controlled locations. In standard laboratory environments (20-24 °C)²⁵, both housing and data collection take place below the thermoneutral zone of mice (26-34 °C)²⁶⁻²⁸. The ThermoMaze exploits the animal’s behavioral thermoregulation mechanisms^{29,30} and promotes thermotaxis (i.e., movement in response to environmental temperature)³¹. Searching for a warmer environment, social crowding and nest building are natural behavioral components of heat homeostasis³¹⁻³³. The ThermoMaze allows the experimenter to guide small rodents to multiple positions in a two-dimensional environment. Decreasing the maze floor temperature induces heat-seeking behavior and after finding a warm spot, the animal stays immobile at that spot for extended periods of time, allowing for recording large amounts of neurophysiological data in immobility-related brain states. We report on both behavioral control and hippocampal electrophysiological correlates of heat-seeking activity to illustrate the versatile utility of the ThermoMaze.

Results

Design and Construction of the ThermoMaze

The ThermoMaze is designed to guide small rodents to warm spatial locations in a two-dimensional cold environment, consisting of a box (width, length, height: 20, 20, 40 cm, respectively) made from an acrylic plexiglass sheet (Fig. 1A, top). The floor of the maze is constructed from 25 Peltier elements (40 x 40 x 3.6 mm) that are attached to aluminum water cooling block heatsinks (40 x 40 x 12 mm, n = 25) with heat-conductive epoxy and are insulated from each other by wood epoxy (Fig. 1A, dashed inset). Each Peltier element is controlled by an electrically operated switch (relay) that opens and closes high-current circuits by receiving transistor-transistor-logic (TTL) signals from outside sources (Fig. 1B). Peltier elements can be heated individually up to 30 °C to provide a “warm spot” for the animal when other regions of the floor are under cooling (Fig. 1B, active heating of one Peltier element is shown). The ambient temperature of the maze is controlled by water circulated from the water tank through the water-cooling blocks. We set the floor temperature to either ~25°C (room temperature) or to ~10 °C (cooling, Fig. 1C and Suppl. Fig. 1), but a range of ambient temperatures (5-30 °C) could be employed. The water temperature is monitored by a K-type thermocouple placed inside the water tank (Fig. 1A bottom). The floor temperature of the ThermoMaze is monitored using a thermal camera (FLIR C5) providing continuous registration of real-time temperature changes (Fig. 1A).

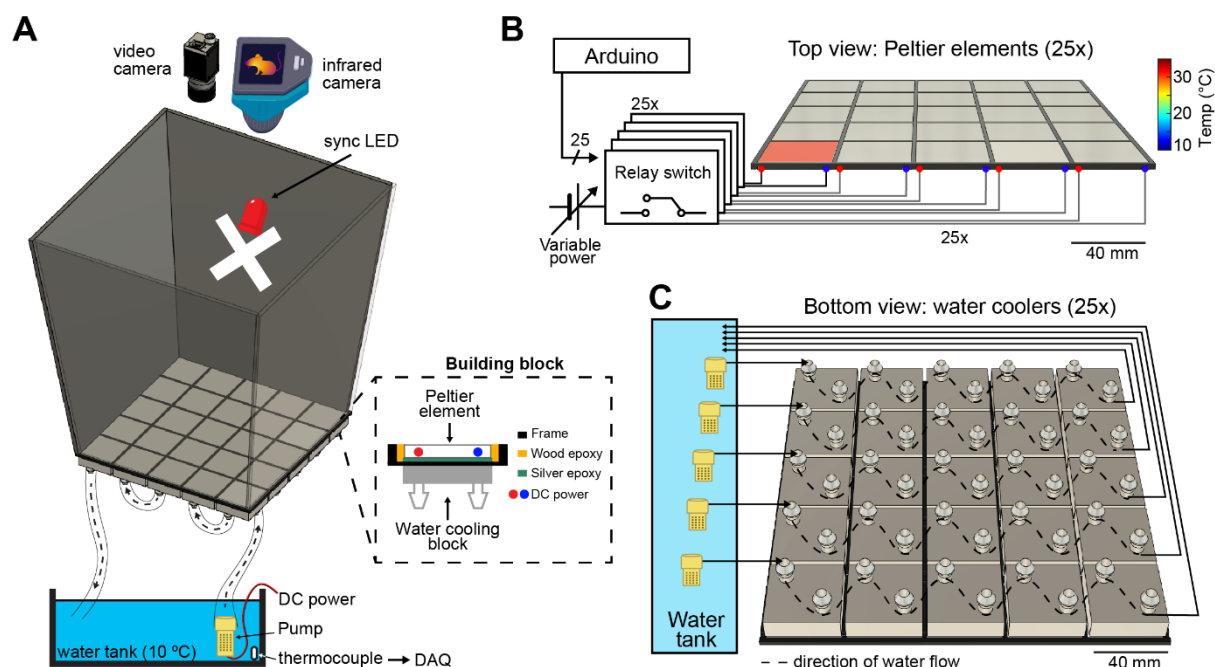


Figure 1. Construction and temperature control of the ThermoMaze. **A)** Schematic of the ThermoMaze. The floor was built using 25 Peltier elements attached to water cooling block heatsinks (building block). The position of the animal and the temperature of the ThermoMaze can be recorded using a video camera and an infrared camera positioned above the box, respectively. An ‘X’ was taped inside the maze as an external cue below the camera synchronizing LED. Water circulates through the water cooling heatsinks using a water pump submerged in a water tank (one row of heatsinks is attached to one pump). The temperature of the water tank is monitored and recorded using a thermocouple (white symbol inside water tank, DAQ – analog input of the data acquisition system). Peltier elements are connected to a power supply (red and blue dots represent the anode and cathode connection). **B)** Circuit diagram and schematic of Peltier elements ($n = 25$), viewed from the top. TTL pulses generated by an AVR-based microcontroller board (Arduino Mega 2560) close a relay switch connected to a variable voltage power source. Each Peltier element can be independently heated (surface temperature depends on applied voltage and temperature difference between hot and cold plate of Peltier element). **C)** Schematic of the water circulation cooling system, viewed from the bottom of the floor (each Peltier element has its own water-cooling aluminum heatsink, shown in silver, $n = 25$). Five submerging DC pumps are used to circulate water across 25 heatsinks (dashed lines show the Peltier elements connected to one pump). The temperature of the heatsink is transferred to the Peltier element passively through the silver epoxy resulting in passive cooling of the floor of the ThermoMaze.

Prior to the experiments, the thermal camera, which continuously measures the surface temperature of the floor of the ThermoMaze is calibrated by thermocouples placed directly on Peltier elements (Fig. 2). The accuracy of the FLIR 5C infrared camera is ± 3 °C. With proper calibration and attention to emissivity (an object’s ability to emit rather than reflect infrared energy) the margin of error can be less than 1 °C³⁴.

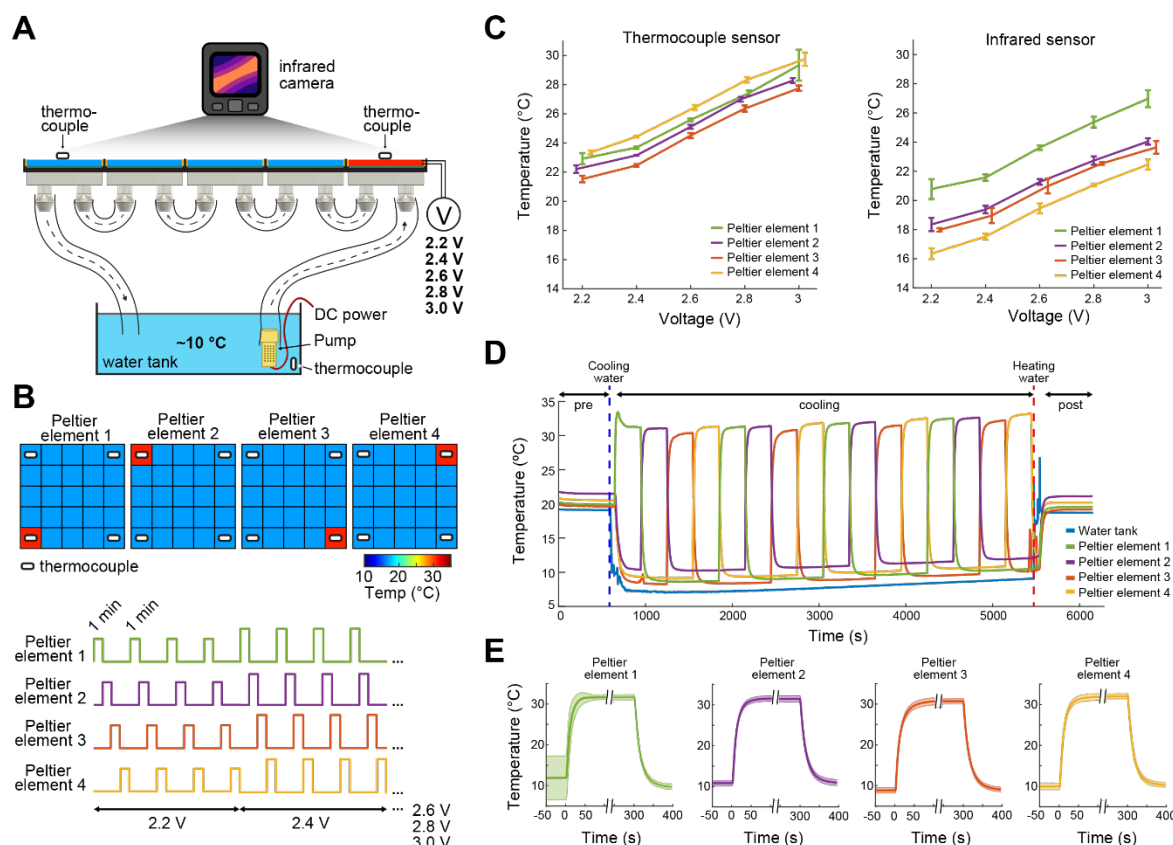


Figure 2. Calibration of the ThermoMaze temperature regulation. **A)** Side view of the ThermoMaze. Prior to animal experiments, we calibrated the heating and cooling performance of the Peltier elements and temperature measurement. We attached thermocouples (white symbols) to the surface of the Peltier elements serving as the ground-truth for calibrating the infrared camera placed above the ThermoMaze. Different voltage levels were used for the calibration (2.2, 2.4, 2.6, 2.8 and 3V) while the water tank temperature was kept constant. **B)** Top: four Peltier elements used in later experiments are chosen for calibration (four corners). Bottom: one minute heating was repeated four times at each voltage level. **C)** Simultaneously recorded temperature by thermocouples (left) and infrared camera (right). Increasing voltages induced increased heating ($n = 4$ trials per intensity, mean \pm SD are shown). While the temporal dynamics yielded similar results between the two systems, we found $\sim 4^\circ\text{C}$ offset between infrared and thermocouple-measured signals. **D)** Temperature changes of four Peltier elements used during an emulated behavioral session (without any animal subject) tracked by thermocouples. **E)** Temporal dynamics of temperature changes at the four Peltier elements during active heating and following passive cooling. The temperature reaches steady state within 31 ± 10.3 seconds (mean \pm SD, $n = 4$ trials across 4 Peltier elements).

Mice seek out hidden warm spots in the ThermoMaze

To illustrate the novel advantages of the ThermoMaze on behavior and brain activity, we tested 11 mice ($n = 3$ male and 8 female mice) with silicon probe recordings from the hippocampus (Suppl. Table 1). One wall was marked by a prominent visual cue (black tape and blinking light-emitting diode; LED) to provide a distinct spatial cue in the box (Fig. 1A)³⁵. On each experimental day, the mouse was placed in the ThermoMaze and allowed to explore it for 10 min at room temperature (“Pre-cooling” sub-session; Figure 3A). Next, the ThermoMaze

temperature was decreased to around 14 °C for 80 min and four Peltier elements (“warm spots”; typically, in the corners) were sequentially and repeatedly turned on and heated up to 30 °C. One Peltier element was turned on for 5 minutes in a sequential order (1-2-3-4) and the sequence was repeated four times (“Cooling” sub-session; Figure 3B). The Cooling sub-session was divided into 5-minute “warm spot epochs” for analysis. The daily experimental session ended with a “Post-cooling” sub-session (free exploration at room temperature for 10 min). In addition, all mice were recorded in the home cage both before and after the experimental session (Fig. 3A). During Pre- and Post-cooling sub-sessions, the animal explored the maze relatively evenly with a moderate movement speed (Figure 3B-D), although thigmotaxis was the dominant pattern, with corners as highly preferred sites of both movement and immobility (Suppl. Fig. 2). The animals readily found the location of the warm spot after a few training sessions (median = 3). Changing the warm spot locations during Cooling induced locomotion until the mouse found another warm spot and stayed on it for prolonged periods (Figure 3B and C, n = 17 sessions in 7 mice). Duration spent on the warm spot roughly followed a bimodal distribution with a median = 2.85 minutes (Suppl. Fig. 2A). Compared to Pre and Post sub-sessions, during Cooling, mice spent a smaller proportion of time in locomotion (Pre: 40 ± 19%, Post: 34 ± 16%, Cooling: 23 ± 12%, mean ± SD, defined as speed > 2.5 cm/s, n = 20 sessions from 7 mice; Figure 3D) and more time in immobility (Pre: 59 ± 19%, Post: 66 ± 16%, Cooling: 76.74 ± 12.41%, mean ± SD, defined as speed ≤ 2.5 cm/s; n = 20 sessions from 7 mice; Figure 3D). The mice spent most of the time in the corners of the ThermoMaze where heat was provided (Suppl. Fig. 2B), compared to Pre- and Post-cooling (Figure 3C). Once the heating of the Peltier element was turned off, the animal quickly left the warm spot (median duration = 12.99 s, n = 20 sessions from 7 mice; Figure 3E) and searched for a new source of warmth. Mice increased their speed from 0 cm/s to 2.5 cm/s within 12.28 s after a warm spot was turned off (median, n = 20 sessions from 7 mice; Figure 3F) and found the new warm spot within 23.45 s (median, n = 20 sessions from 7 mice; Fig. 3G). In two additional male mice, we examined brain temperature changes during the Cooling sub-session by implanting a thermistor in the hippocampus (Suppl. Fig. 3A). In support of previous findings, we found brain state-dependent fluctuation of brain temperature (Suppl. Fig. 3B)^{36–38}. However, cooling the environment *per se* did not correlate with brain temperature changes (Suppl. Fig. 3C-E), confirmation that brain temperature is strongly regulated and is largely independent of the ambient temperature³⁸. The ThermoMaze provides an affordance for mice to select their environmental temperature through the activation of behavioral thermoregulation³⁹. We also quantified the changes in LFP (1-40 Hz) to test whether the brain state of the animal was similar in the ThermoMaze and home cage during wakeful periods. We did not find significant changes in these frequencies (Suppl. Fig. 4).

One of the objectives in developing the ThermoMaze was to induce immobility at several locations repeatedly and for extended periods. To confirm that this objective was achieved, we ran control sessions with the same duration as the Cooling sub-session but at room temperature (80 minutes; Suppl. Fig. 5). Under room temperature conditions (3 sessions in 3 mice), mice first explored the ThermoMaze and settled in one of the corners for an extended period. Although mice spent a similar total amount of time immobile under both conditions, the spatial distribution of immobility durations was more uniform in the Cooling sub-session (Suppl. Fig.

5) because the ThermoMaze paradigm forced the animals to leave their chosen spot and move to the experimenter-designated locations, i.e., the new warm spots away from the corner (Suppl. Fig. 6).

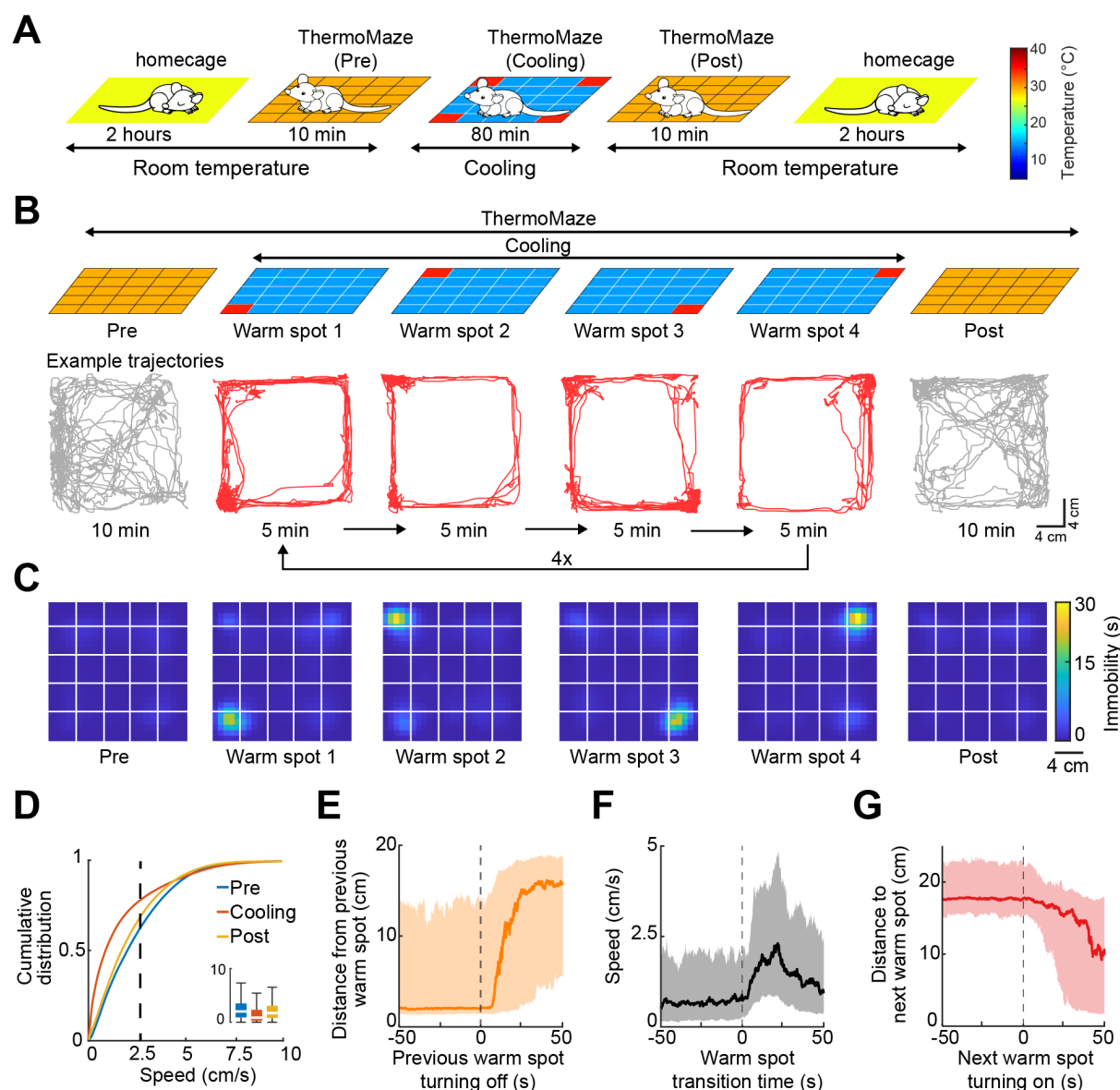


Figure 3. Mice track and stay immobile on hidden warm spots in the ThermoMaze. **A)** Five sub-sessions constituted a daily recording session: (1) rest epoch in the home cage, (2) pre-cooling exploration epoch (Pre), (3) Cooling, (4) post-cooling exploration epoch (Post) and (5) another rest in the home cage. **B)** Schematic of temperature landscape changes when the animal is in the ThermoMaze (top) and example animal trajectory (below). During Cooling, one Peltier element always provided a warm spot for the animal (four Peltier elements in the 4 corners were used in this experiment). Each Peltier element was turned on for 5 minutes in a sequential order (1-2-3-4) and the sequence was repeated four times. **C)** Session-averaged duration of immobility (speed ≤ 2.5 cm/s) that the animal spent at each location in the ThermoMaze; Color code: temporal duration of immobility (s); white lines divide the individual Peltier elements; $n = 17$ session in 7 mice). **D)** Cumulative distribution of animal speed in the ThermoMaze during three sub-sessions from 7 mice). Median, Kruskal–Wallis test: $H = 139304.10$, d.f. = 2, $p < 0.001$. **E)** Animal's distance from the previously heated Peltier element site. **F)**

Speed of the animal centered around warm spot transitions. **G)** Animal's distance from the target warm spot as a function of time (red curve: median; time 0 = onset of heating). * $p < 0.05$, ** $p < 0.01$, *** $p < 0.001$. In all panels, box chart displays the median, the lower and upper quartiles. (see Supplementary Table 2 for exact p values and multiple comparisons).

Firing rate maps of hippocampal neurons in the ThermoMaze

Compared to spatial learning and memory paradigms such as the Morris water maze⁴⁰, the ThermoMaze has a non-aqueous environment and thus allows for an easy setup of electrophysiological recording. We recorded neurons from the CA1 hippocampal region by multi-shank silicon probes and separated them into putative pyramidal cells and interneurons (Methods - Unit isolation and classification section). We separated behavioral states (movement or immobility) based on movement speed (speed ≥ 2.5 cm/s = movement and speed < 2.5 cm/s = immobility).

To construct spike count maps for comparing sub-sessions, the ThermoMaze was divided into 25 x 25 bins and the number of spikes emitted by a neuron in each bin was counted and normalized by the time the mouse spent in each spatial bin. The impact of cooling during movement (theta state) was compared by calculating the correlation coefficients between Pre and Post, Pre and Cooling, and Cooling and Post spike count maps (Suppl Fig. 7A). The correlation coefficients decreased significantly across all sub-sessions, with the largest change observed between Pre-cooling and Post-cooling spike count maps in the experimental mice (Suppl Fig. 7B). Thus, the Cooling sub-session in the ThermoMaze induced a moderate decorrelation of pyramidal cells' rate maps, potentially explained by place field remapping upon changing environmental sensory cues (here, temperature gradient)⁴¹. Such observation constrained our ability to decode spatial information from the spiking activity during SWP-Rs in the Cooling sub-session using firing rate maps constructed during Pre- and Post-cooling sub-sessions⁴², because the Bayesian decoding approaches have an underlying assumption that the spatial representation (tuning functions, or rate maps) is temporally stable.

Because the ThermoMaze is a relatively small enclosure, one possibility is that CA1 neurons encode less spatial information and only a small number of place cells could be found. Therefore, we identified place cells in each sub-session separately (see more details in the Method section for place cell definition, Suppl. Fig. 8). We found 40.90%, 45.32%, and 41.26% of pyramidal cells to have place fields in the Pre-cooling, Cooling, and Post-cooling sub-sessions respectively. Furthermore, we found that, on average, 17.36% of pyramidal neurons passed the place field criteria in all three sub-sessions in a daily session. Therefore, the decorrelation of spatial firing maps across sub-sessions cannot be explained by poor recording quality or weak neuronal encoding of spatial information but is potentially due to changes in environmental cues.

In principle, comparison of place maps during the first and last 10 min of a 100 min session at room temperature should serve as controls. However, at room temperature mice "designate" one of the corners as home base after a few minutes of exploration and stay in that corner for the rest of the session (Suppl. Fig. 5A). Thus, exploration of the maze at the end of the session was not available.

Place-selective neuronal firing during SPW-Rs at experimenter-designated locations

As expected, SPW-Rs occurred predominantly in the corners (Fig. 4A), where the mice spent most of their time resting (Fig. 3C). Compared to room-temperature control sessions where animals spent most of their time in one corner, the spatial distribution of SPW-Rs in the Cooling sub-session was more uniform (Suppl. Fig. 5A-D), indicating that the ThermoMaze paradigm successfully biased where SPW-Rs were generated. The duration and amplitude of SPW-Rs were comparable in the ThermoMaze and the home cage (Fig. 4 B, C), whereas the mean peak frequency of SPW-Rs were significantly lower (Fig. 4D). This decrease can be explained by the lower brain temperature during sleep, a state in which the animals spent most of their time in the home cage³⁶.

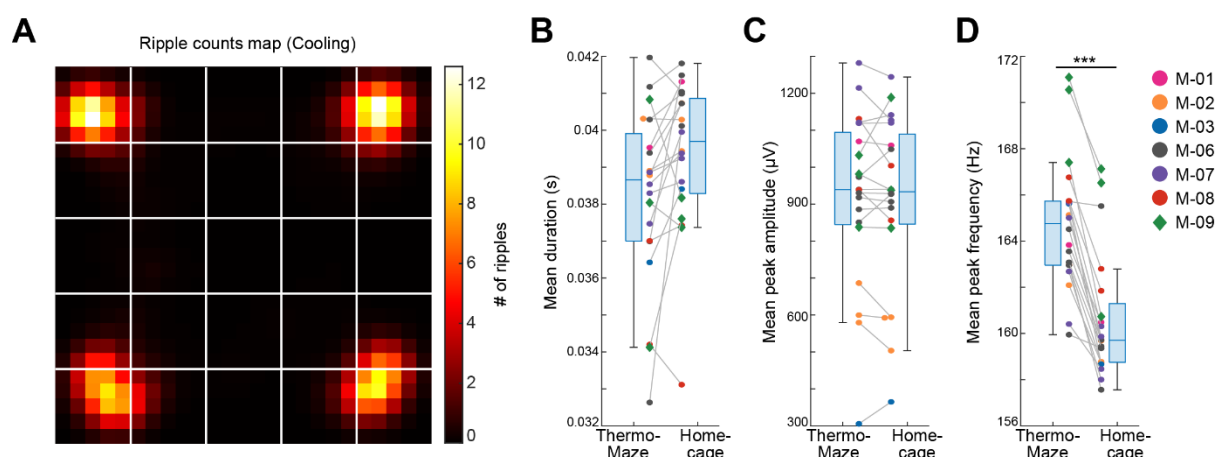


Figure 4. Location-specific distribution of SPW-R in the ThermoMaze **A)** Spatial map of the number of SPW-Rs during the Cooling sub-session averaged across all sessions (Color code: average number of SPW-Rs per session at each location). Session-average number of SPW-Rs during Cooling was 627.3 (corresponding to 0.136 Hz). **B-D)** Boxplots of SPW-R properties in ThermoMaze and in the home cage ($n = 19$ sessions in $n = 7$ mice). **B)** Mean ripple duration in seconds (s; $p = 0.108$). **C)** Mean ripple amplitude in μ V ($p = 0.9$). **D)** Mean ripple peak frequency in Hz ($p < 0.001$). Dots (females) and diamonds (males) of the same color represent the same animal.

To quantify spatial tuning features of neuronal firing during SPW-Rs in the ThermoMaze during the Cooling sub-session, we defined a metric referred to as “spatial tuning score” (STS). We first binned the floor of the ThermoMaze into four quadrants (2x2). For each neuron, we calculated its average firing rate within SPW-Rs in each quadrant. STS was then defined by the firing rate in the quadrant with the highest within-SPW-R firing rate divided by the sum of the within-SPW-R firing rates in all four quadrants (yielding a value between 0 and 1; Fig. 5A). To test the significance of STS, we compared the STS values with their shuffled versions by randomly assigning one of the four quadrants to each SPW-R. The distribution of the STS in actual SPW-Rs was significantly higher compared to shuffled controls (Fig. 5B). Additionally, pyramidal cells exhibited higher STSs compared to interneurons (medians: pyramidal cells = 0.3432; interneurons = 0.2934; one-sided Wilcoxon rank sum test, $p < 0.001$). In summary, both excitatory and inhibitory neuronal populations exhibit place-selective firing during SPW-Rs, while the excitatory neurons demonstrate a stronger place-specific firing.

To quantify how well CA1 neurons encode spatial information during SPW-Rs at the population level, we carried out a Bayesian decoding analysis to read out the current position of the animal from spiking activity⁴². We constructed firing rate map templates using spikes within SPW-Rs in the training dataset and determined animal positions that maximized the likelihood of observing the spike train during SPW-Rs in the testing dataset (see Method). Spiking activity during SPW-Rs reliably identified the quadrant that the animal was in above chance level (Figure 5C, D) irrespective of whether we incorporated the spatial distribution priors into the decoder in an example session (Figure 5C) or used a uniform prior (Figure 5D).

To relate the spatial content of spikes during SPW-Rs and locomotion, we examined whether the same or different groups of neurons contributed to the place-specific firing during SPW-R and locomotion by calculating the firing rate ratios within the preferred quadrant versus all quadrants. These ratios during SPW-Rs and movement were positively correlated (Fig. 5E; $n = 1150$ pyramidal cells in 20 sessions from 7 mice), suggesting that place cells⁴³ during movement preserved their spatial properties during SPW-Rs (see also Suppl. Fig. 9 for further analysis and findings on interneurons).

Finally, we tested whether the preservation of spatial features of neuronal spiking also holds at the population level by constructing population vectors separately during movement and SPW-Rs. We then computed the pairwise correlation coefficients between these two conditions. As was the case for individual pyramidal cells, population vectors for the same quadrant during movement were similar to those during SPW-Rs (Figure 5F). Overall, these findings support and extend the observation that spiking activity during SPW-Rs continues to be influenced by the animal's current position⁴⁴.

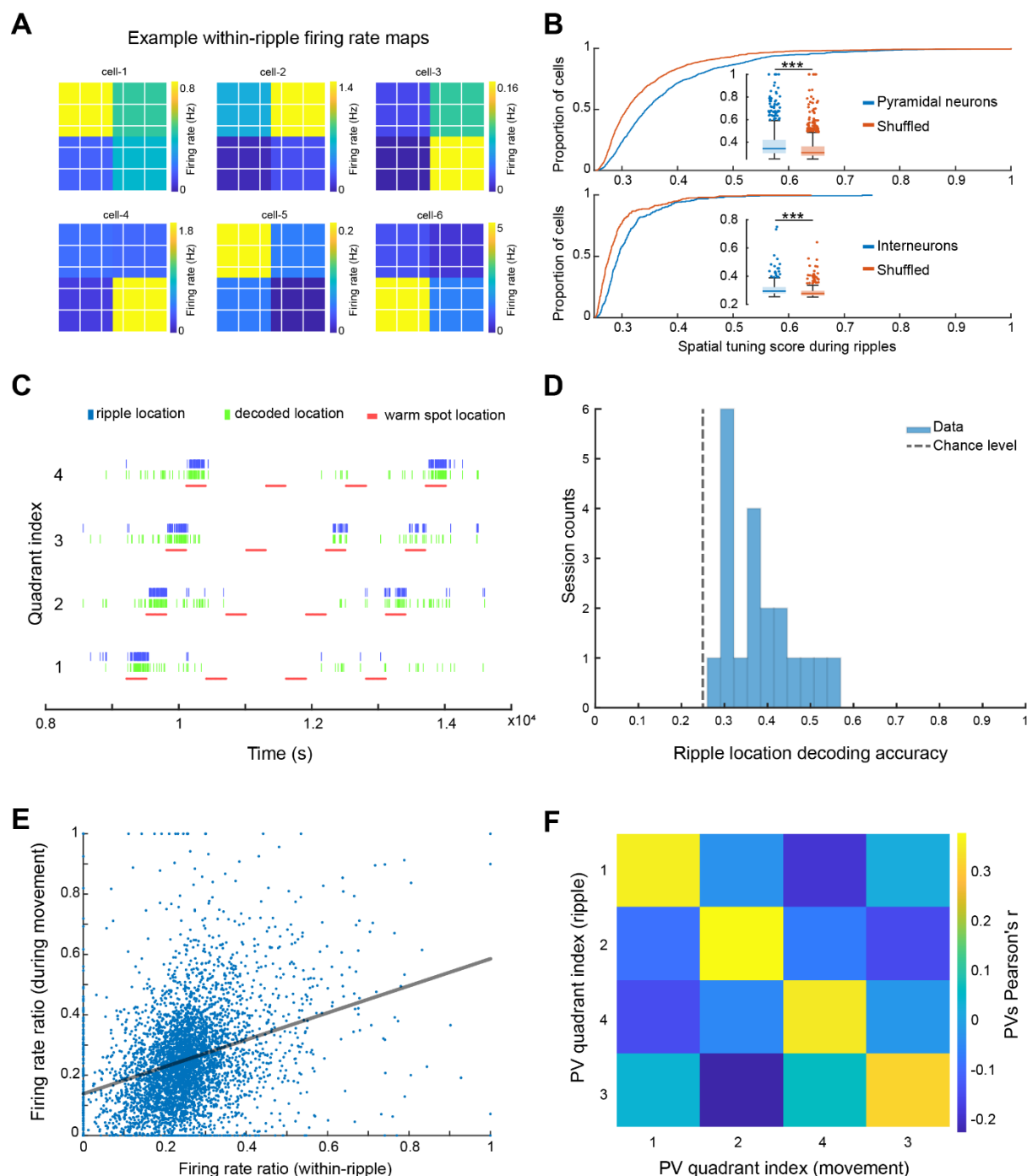


Figure 5. Spikes of CA1 pyramidal neurons during awake SPW-Rs are spatially tuned. **A)** Within SPW-R firing rate maps (ThermoMaze divided into four quadrants) of 6 example cells with high within SPW-R spatial tuning score (STS; from left to right, top to bottom, STS= 0.458, 0.639, 0.592, 0.672, 0.655, 0.660 respectively). Color represents within SPW-R firing rate (in Hz) of the neuron in each quadrant of the ThermoMaze. **B)** Cumulative distribution of spatial tuning scores of pyramidal neurons (top; $n = 1150$; $p < 0.001$) and interneurons (bottom; $n = 288$; $p < 0.001$) during SPW-Rs. Chance levels were calculated by shuffling the quadrant identity of the SPW-Rs. One-sided Wilcoxon rank sum tests. **C)** Bayesian decoding of the mouse's location (quadrant of the ThermoMaze) from spike content of SPW-Rs in an example session (blue: actual ripple location; green: decoded locations; red: locations of the warm spot; session decoding accuracy = 0.65; chance level = 0.26). **D)** Histogram of session Bayesian decoding accuracies of ripple locations using spiking rate maps constructed during ripples as

templates (with a uniform prior and a 100-fold cross-validation; $P < 0.001$). One-sample t-test. **E)** Firing rate ratios of pyramidal cells constructed during SPW-Rs and movement are positively correlated (Pearson's $r = 0.321$, $p < 0.001$). The firing rate ratio measures the firing rate of a cell in one quadrant versus the sum of its firing rates in all four quadrants under a specific condition (within-ripple or during movement). **F)** Matrix of the pairwise correlation coefficient between each pair of firing rate ratio population vectors constructed during SPW-Rs and movements in different quadrants (x and y axes). Color represents Pearson's r .

To test specifically whether perceptual sensing of environmental features is critical in position-specific firing of neurons during SPW-Rs, we prolonged the duration of warm spots. After the Pre-cooling sub-session, the ThermoMaze temperature was decreased to 16 °C for 80 min and two Peltier elements were heated alternately to 30 °C for 20 min (Figure 6A). As expected, mice spent most of the time immobile on the warm spots (Figure 6A,B). Similar to the 5-minute protocol (Fig. 4A), SPW-Rs occurred predominantly on the warm spots (Fig. 6C). The increased duration of stay on the warm spot facilitated the occurrence of sleep, as quantified by our brain state scoring algorithm (Fig. 6D, SPW-Rs). REM sleep was not detected since REM state typically emerges after 20-30 min of NREM episodes⁴⁵. Mice spent a higher fraction of their time in sleep during the 20 min, compared to the 5 min sub-session ($p = 0.003$, $n = 19$ sessions in 7 mice and $n = 7$ sessions in 4 mice, Suppl. Table 1). The average inter-NREM interval was 1000 seconds (Fig. 6F, $n = 7$ sessions in 4 mice). Comparing the population vector similarity of waking SPW-Rs vs. NREM SPW-Rs to movement vs. waking SPW-Rs and movement vs. NREM SPW-Rs, we found that place-specific coding during SPW-Rs persists into sleep, and we observed the highest correlation when comparing SPW-Rs during different brain states than when comparing SPW-Rs and movement (Fig. 6G). These findings further support the view that sensory inputs during waking SPW-Rs can affect the spiking content of SPW-Rs.

Since sleep occurred on the warm spots during the prolonged stays, we also tested our hypothesis that the difference in the mean ripple peak frequency (Fig. 4D) between the home cage and ThermoMaze was due to the sleep vs. non-sleep states. We compared the ripple peak frequency that occurred during wakefulness and NREM epochs in the home cage and ThermoMaze ($n = 7$ sessions in 4 mice). We found that the peak frequency of the awake ripples was higher compared to both home cage and ThermoMaze NREM sleep (one-way ANOVA with Tukey's posthoc test; ripple frequencies were: 171.63 ± 11.69 , 172.21 ± 11.86 , 168.19 ± 11.10 and 168.26 ± 11.08 Hz, mean \pm SD for home cage awake, ThermoMaze awake, home cage NREM and ThermoMaze NREM conditions, $p < 0.001$ between awake and NREM states).

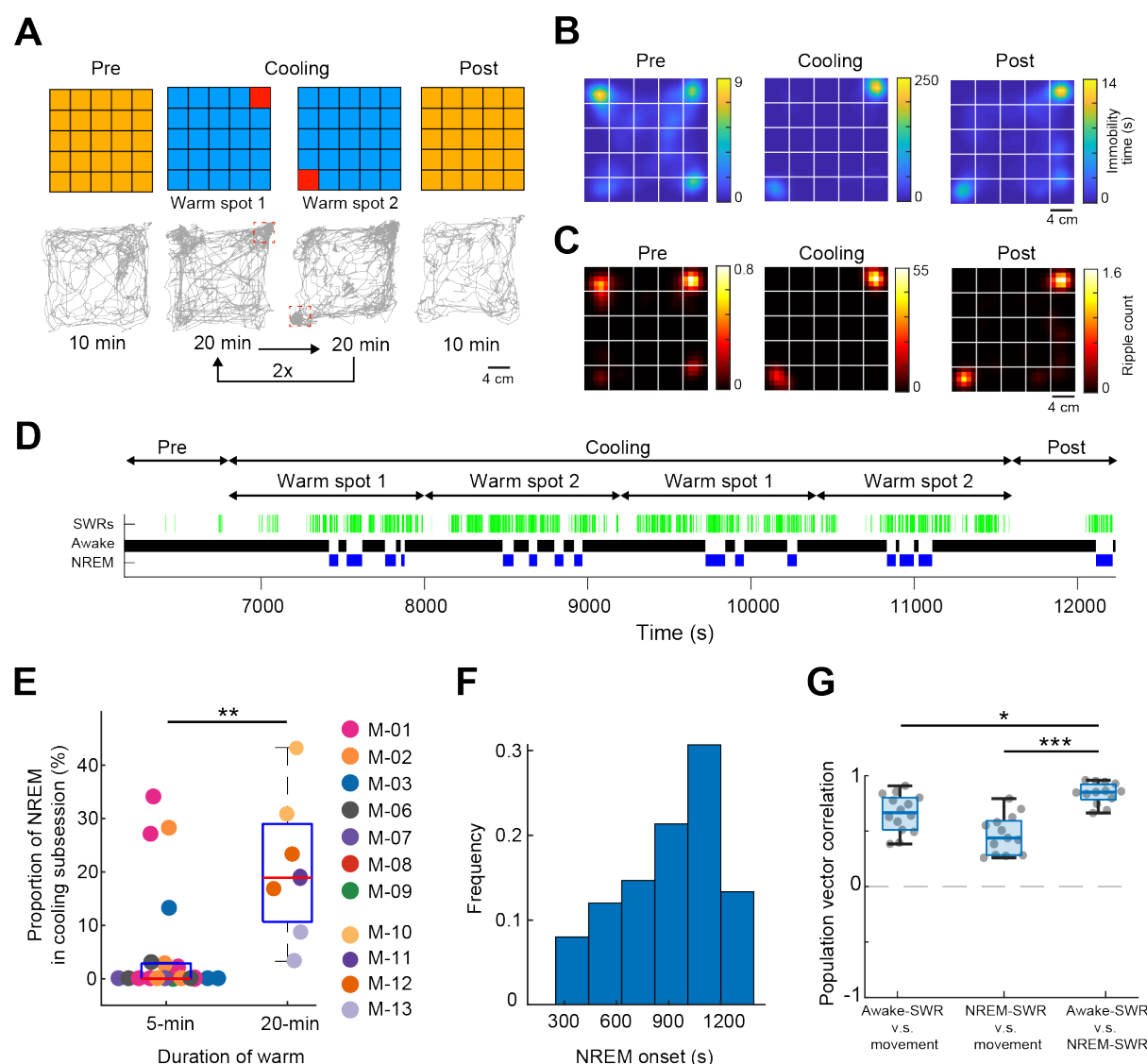


Figure 6. Mice sleep at experimenter-defined locations. **A)** Schematic of ThermoMaze with warm spot locations (top) and the trajectory of an example animal (bottom; red rectangles correspond to the location of warm spots). During Cooling, one Peltier element was turned on for 20 min followed by another (1-2) and the sequence was repeated two times. **B)** Session-averaged duration of immobility (speed ≤ 2.5 cm/s) at each location in the ThermoMaze; white lines divide the individual Peltier elements ($n = 7$ sessions, $n = 4$ mice). **C)** Spatial distribution of SPW-R occurrences (color code: average number of SPW-Rs per session at each location, $n = 7$ sessions, $n = 4$ mice). Session-average of SPW-Rs during Cooling was 775 (corresponding to 0.16 Hz). **D)** Long duration of heating allowed for NREM sleep occurrence during Cooling sub-session in an example session. Brain state changes⁴⁵ are shown together with SPW-Rs (green ticks). Note that NREM sleep occurs in the second half of the 20-min warming. **E)** Mice spent a larger fraction of time in NREM during 20 min Cooling sub-session compared to the 5 min task variant ($p = 0.003$, $n = 19$ sessions in 7 mice and $n = 7$ sessions in 4 mice). **F)** Mice typically spent ~ 1000 seconds awake between NREM epochs. **G)** Box charts of Pearson's correlation coefficients between population vectors of CA1 pyramidal neurons constructed during awake SPW-Rs, movement, and NREM SPW-Rs. Median, Kruskal–Wallis test: $H = 20.7$, d.f. = 2, $p < 0.001$ (pairwise comparison: $*p = 0.037$ and $***p = 1.6 \times 10^{-05}$).

Discussion

To investigate the importance of brain state transitions in a controlled manner, we developed the ThermoMaze, a behavioral paradigm that allows for the collection of large amounts of physiological data while the animal rests at distinct experimenter-controlled locations. Since the paradigm exploits natural behavior, no extensive training or handling is necessary. We demonstrate that mice regularly explore a cold environment until a warm spot is identified. They spend most of the time in a warm spot and even fall asleep, thus exhibiting a high degree of comfort. We exploited the long immobility epochs following exploration and showed how neurons active during hippocampal sharp wave ripples (SPW-R) replay waking experience. The ThermoMaze will allow for detailed studies of brain correlates of preparatory-consummatory transitions and open new options for studying temperature homeostasis.

Warmth-seeking homeostatic behavior

There is a renewed interest in exploiting natural learning patterns, as opposed to training animals for performing complex arbitrary signal-action associations^{46–53}. In poikilotherm animals (species whose internal temperature varies with environmental temperature), energy homeostasis is one of the most fundamental homeostatic processes. Heat homeostasis involves multiple levels of coordination from cellular to systems, from peripheral to central^{54,55}. To maintain core body temperature, thermogenic tissues rapidly increase glucose utilization by brown adipose tissue and shivering by skeletal muscle^{56,57}. The hypothalamic preoptic area (POA) is regarded as the most important thermoregulatory “center” in the brain^{58,59}. Connecting this area of research to learning, the POA is bidirectionally connected with the limbic system and multiple cortical areas which assist both online maintenance of body temperature and preparing the body for future expected changes (“allostasis”)^{23,60,61}. These allostatic mechanisms induce exploratory behavior, searching for a warmer environment^{62,63}. A location that provides a warm shelter needs to be remembered and generalized for future strategies. Our paradigm offers means to investigate exploratory-consummatory transitions, wake-sleep continuity in the same physical location and, in the reverse direction, the physiological processes that evaluate discomfort levels, motivate behavioral transition from rest to exploration, and the circuit mechanisms that give rise to overt behaviors.

Mice, and rodents in general, are acrophobic and agoraphobic and tend to avoid open areas. Instead, they tend to move close to the wall and spend most of their non-exploration time in corners⁶⁴. Thus, while we were able to train mice to seek out and stay in warm spots in the center of the maze after extensive training, their evolutionary “counter-preparedness”⁴⁸ to stay in predator-prone open areas competed with the reward of warming. While these trained mice did stay transiently in the central warm spot, they spent more time returning to the corners. Our mice were on a normal day-light schedule thus their training during the day coincided with their sleep cycle. This explains why after 5-10 min spent on the safe and temperature-comfortable corner warm spots they regularly fell asleep. Yet, we noticed that mice did not simply transition from walking to immobility but, instead, even after finding the warm spot they regularly and repeatedly explored the rest of the maze before returning to the newly identified home base. By changing the temperature difference between the environment and the warm spot, it will be possible to generate psychophysical curves to quantify the competition

between homeostatic and exploratory drives in future experiments. These measures, in turn, could be used to study the impact of perturbing peripheral and central energy-regulating mechanisms.

For several applications, there is no need to tile the entire floor of the maze with Peltier elements. For example, a radial-arm maze with cooled floors or placed in a cold box can be equipped with heating Peltier elements at the ends of maze arms and center, allowing the experimenter to induce ambulation in the 1-dimensional arms, followed by extended immobility and sleep at designated areas. In a way, the ThermoMaze is analogous to the water maze⁴⁰, also an avoidance task, but many more trials can be achieved in a single session and without the inconvenience of a wet environment.

SPW-R spiking content is biased by current position of the animal and depends on brain state

We demonstrate the utility of the ThermoMaze for addressing long-standing questions in hippocampal physiology. Preparatory and consummatory behaviors in the hippocampus are associated with theta oscillations and SPW-Rs, respectively¹⁰. SPW-Rs also occur during NREM sleep but studying the differences between waking and sleep SPW-Rs has been hampered by the paucity of SPW-Rs in typical learning paradigms^{21,22,65–68}. Neural activity during SPW-Rs has been shown to replay activity patterns observed during previous spatial navigation experiences^{21,44,65} and can even be predictive of activity during future experiences^{69–71}. However, the extent to which SPW-R spiking context is biased by the current position of the animal is less known, as systematic control of position during rest/sleep has posed difficulty. The ThermoMaze enables the experimenter to control the animal's position during SPW-R states. In agreement with previous studies^{44,66,68}, we found that neurons whose place fields overlapped with the quadrant of the maze had a higher participation probability in SPW-Rs occurring at that location compared to other neurons. This observation supports the notion that waking replay events can be biased by perceiving features of the surrounding environment⁴⁴. However, when the mouse fell asleep at the same location this relationship was weakened but did not disappear. Another potential explanation for the decreased correlation between sleep SPW-R and waking exploration is the deterioration of replay as the function of time¹⁵. Alternatively, the persisting significant correlation between sleep SPW-Rs and previous exploration may also indicate that factors other than the perception of the animal's vicinity are responsible for sleep replay^{71–73}. Continuity of waking experience replay in waking and sleep SPW-Rs have been hypothesized previously but not yet tested⁷⁴. Using the ThermoMaze, this and other related questions can now be addressed quantitatively.

441 **ACKNOWLEDGEMENTS**

442 We thank Daniel Levenstein for useful comments on the manuscript. We thank Yiyao Zhang,
 443 Anna Maslarova and Leeor Alon for their help with different aspects related to the experiments.
 444 Supported by MH122391, and U19NS107616.

445 **Author contributions:** MV designed the ThermoMaze, MV and YZ performed surgeries, MV,
 446 YZ and AR collected data, MV, YZ, KM and RH processed data. GB, MV, YZ, KM, RH and
 447 wrote the manuscript.

448

EXPERIMENTAL METHODS

Animals and surgery

All experiments were approved by the Institutional Animal Care and Use Committee at New York University Langone Medical Center. Animals were handled daily and accommodated to the experimenter and the ThermoMaze before the surgery and electrophysiological recordings. Mice (adult female $n = 8$, 22 g and male $n = 5$, 26 g) were kept in a vivarium on a 12-hour light/dark cycle and were housed two per cage before surgery and individually after it. Atropine (0.05 mg/kg, s.c.) was administered after isoflurane anesthesia induction to reduce saliva production. The body temperature was monitored and kept constant at 36–37 °C with a DC temperature controller (TCAT-LV; Physitemp, Clifton, NJ). Stages of anesthesia were maintained by confirming the lack of a nociceptive reflex. The skin of the head was shaved, and the surface of the skull was cleaned by hydrogen peroxide (2%). A custom 3D-printed baseplate⁷⁵ (Form2 printer, FormLabs, Sommerville, MA) was attached to the skull using C&B Metabond dental cement (Parkell, Edgewood, NY). The location of the craniotomy was marked and a stainless-steel ground screw was placed above the cerebellum. Silicon probe (Suppl. Table 1) attached to a metal microdrive⁷⁶ was implanted into the dorsal CA1 of the hippocampus (2 mm posterior from Bregma and 1.5 mm lateral to midline) and a copper mesh protective cap was built around the probe. Animals received ketoprofen (5.2 mg/kg, s.c.) at the end of the surgery and on the following two days. Each animal recovered at least 5 days prior to experiments. The electrophysiology data was digitized at 20000 samples/s using an RHD2000 recording system (Intan technologies, Los Angeles, CA). The number of recorded sessions from each animal is summarized in Supplementary Table 1.

Construction of ThermoMaze

The ThermoMaze is a box (width, length, height: 20, 20, 40 cm, respectively), made from acrylic plexiglass sheet (8505K743, McMaster, Elmhurst, IL). The floor of the maze was constructed from 25 Peltier elements (40, 40, 3.6 mm, Model: TEC1-12706, voltage: 12V, U_{max} (V): 15V, I_{max} (A): 5.8A, $\Delta T_{max}(Q_c=0)$: up to 65 °C). Each Peltier element was glued inside a custom 3D-printed frame (file can be downloaded from https://github.com/misiVoroslakos/3D_printed_designs/tree/main/ThermoMaze) using dental cement (Unifast LC, GC America, Alsip, IL) and wood epoxy (Quick-Cure, product number: BSI201, Bob Smith Industries, Atascadero, CA). Once Peltier elements were secured in the 3D-printed frame, an aluminum water cooling block heatsink (40, 40, 12 mm; a19112500ux0198, Amazon.com) was attached to each Peltier element using heat-conductive epoxy (8349TFM, MG Chemicals, Ontario, Canada). A variable voltage source (E36102A Power Supply, Keysight Technologies, Santa Rosa, CA) was attached to four Peltier elements using a relay system (4-Channel Relay Module, product number: 101-70-101, SainSmart, Lenexa, KS). The relays were controlled by an Arduino Mega (Arduino Mega 2560 Rev3) running a custom written code. Five aluminum water cooling block heatsinks were connected together using silicon tubes (5/16" ID x 7/16" OD, product number: 5233K59, McMaster, Elmhurst, IL). One of the five heatsinks was connected to a mini submersible electric brushless water pump (240L/H, 3.6W, Ledge, ASIN: B085NQ5VVJ) using silicon tubes and another one was routed to the water tank. We used 5 water pumps to circulate water through the 25

cooling blocks. The water pumps were placed inside a water tank (40, 40, 60 cm acrylic box) and were powered using a DC power supply (E3620A, Keysight Technologies, Santa Rosa, CA). The temperature of the water tank was monitored by a K-type thermocouple (5SC-TT-K-40-72, Omega, Norwalk, CT) attached to a handheld thermometer (HH800, Omega, Norwalk, CT) and recorded by a K-type thermocouple (5SC-TT-K-40-72, Omega, Norwalk, CT) attached to an AD595 interface chip (1528-1407-ND, Digi-Key, Thief River Falls, MN) connected to an analog input of the RHD2000 USB Eval system (Intan Technologies, Los Angeles, CA). To monitor the floor temperature of the ThermoMaze, a thermal camera (C5, Flir, Thousand Oaks, CA) was used.

Behavior

The ThermoMaze setup provides a customized temperature landscape, which the animal can freely explore and choose where to settle. Without any training or shaping, a mouse will search and find the unmarked warm spot and stay on it for extended periods due to thermotaxis (movement towards locations with preferred temperature around 26–29°C; Figure 3)^{29,30}. When the heating Peltier element is turned off, the animal quickly leaves the spot and explores the maze again until it finds another warm spot.

On each experimental day, the mouse is taken from the animal facility during their light cycle. The animal is first recorded in its home cage for 1-2 hours (pre-home). It is then transferred into the ThermoMaze under room temperature to freely explore for 10 minutes (Pre-cooling). During the Pre-cooling sub-session, the water circulation system is circulating room temperature water, and the Peltier elements are not activated. After the Pre-cooling sub-session, 4 kg of ice and two ice packs (25201, Igloo) are added into the water tank while the animal remains in the ThermoMaze. Within 1 minute, the temperature of the water in the tank stabilizes at 10-13 °C. We then turn on the pump to cool down the ThermoMaze setup (it takes ~120 seconds to cool down the floor to 10-13 °C). At the same time, the Arduino-controlled Peltier element heating system is turned on to heat one of the four 4 x 4 cm² for 5 minutes, followed by another Peltier device in a fixed sequence (Fig. 2). Such sequence is repeated four times (total of 80 min) during a Cooling sub-session. After the sub-session, the animal explores again at room temperature for 10 minutes (Post-cooling sub-session). To increase the temperature back to ~20 °C, the ice packs are removed, and 6.5 L of 55 °C water is added into the tank. The temperature in the ThermoMaze returns to room temperature within 2 minutes. After the Post sub-session, recording of electrophysiological activity continues in the home cage for an additional 1–2 hours (post-home cage; Fig. 3A).

To quantify the behavior of the animal within the ThermoMaze, video is recorded using a Basler camera (a2A2590-60ucBAS Basler ACE2) using the mp4 format with a framerate of 25 Hz. TTL pulses are sent from the camera to the Intan recording system to synchronize the video and the electrophysiological recordings. The animal's location is detected within a 25x25 cm region of interest (ROI), using a custom-trained DeepLabCut neural network⁷⁷. Detections with a likelihood below 0.5 are discarded. The occasionally missing trajectory detections are filled using MATLAB function “fillmissing” with method “pchip” which is a shape-preserving piecewise cubic spline interpolation and are then smoothed using a 7th-order one-dimensional

median filter “medfilt1”. The detection quality is visually examined by superimposing the detected animal location in each frame on the video.

Brain temperature measurement

To examine the effects of changing environmental temperature on brain temperature homeostasis, we implanted one male and one female wild-type mice (C57Bl6, 28 g) with a thermistor (Semitec, 223Fu3122-07U015) in the hippocampus (2 mm posterior from bregma and 1.5 mm lateral to midline)³⁶. After 5 days of postsurgical recovery, the animal was placed inside the ThermoMaze and brain temperature and behavior were monitored (n = 5 sessions, each session consisted of pre-home cage, Pre, Cooling, Post and post-home cage epochs).

QUANTIFICATION AND STATISTICAL ANALYSIS

SPW-R detection and properties

SPW-Rs were detected as described previously from manually selected channels located in the center of the CA1 pyramidal layer (https://github.com/buzsakilab/buzcode/blob/master/detectors/detectEvents/bz_FindRipples.m). Broadband LFP was bandpass-filtered between 130 and 200 Hz using a third-order Chebyshev filter, and the normalized squared signal was calculated. SPW-R peaks were detected by thresholding the normalized squared signal at 5×SDs above the mean, and the surrounding SPW-R begin, and end times were identified as crossings of 2×SDs around this peak. SPW-R duration limits were set to be between 20 and 200 ms. An exclusion criterion was provided by manually designating a ‘noise’ channel (no detectable SPW-Rs in the LFP), and events detected on this channel were interpreted as false positives (e.g., EMG artifacts). The ripple detection quality was visually examined by superimposing the detected timestamps on the raw LFP traces in NeuroScope2 software suite⁷⁸.

Sleep state scoring and LFP analysis

Brain state scoring was performed as described in the study by Watson et al.,⁴⁵. In short, spectrograms were constructed with a 1-s sliding 10-s window fast Fourier transform of 1,250 Hz data at log-spaced frequencies between 1 Hz and 100 Hz. Three types of signals were used to score states: broadband LFP, narrowband high-frequency LFP and electromyogram (EMG) calculated from the LFP. For broadband LFP signal, principal component analysis was applied to the Z-transformed (1–100 Hz) spectrogram. The first principal component in all cases was based on power in the low (32 Hz) frequencies. Dominance was taken to be the ratio of the power at 5–10 Hz and 2–16 Hz from the spectrogram. All states were inspected and curated manually, and corrections were made when discrepancies between automated scoring and user assessment occurred.

To quantify the changes in LFP (Suppl. Fig. 4A, B), we detected wakeful periods in both the home cage and the ThermoMaze environments. Average LFP power and coherence spectra were calculated with Welch’s power spectral density method. We used a 4096-point fast Fourier transform (FFT), applied to data during wakefulness (non-continuous 2500 seconds in both environments). To compare immobility periods on the ThermoMaze and the home cage,

we detected rest epochs that lasted at least 2 seconds during wakefulness in both environments. This analysis was performed on a subset of animals ($n = 17$ sessions in 7 mice) that had accelerometer signal available (home cage behavior was not monitored by video). Using these behavior transition timepoints, we calculated the event triggered power spectra for delta and theta band (± 2 s around the transition time).

Unit isolation and classification

A concatenated signal file was prepared by merging all recordings from a single animal from a single day. Putative single units were first sorted using Kilosort⁷⁹ and then manually curated using Phy (<https://phy-contrib.readthedocs.io/>). After extracting timestamps of each putative single unit activity, the spatial tuning properties, identification of 2D place cells and place fields, and participation in SPW-Rs events were analyzed using customized MATLAB (Mathworks, Natick, MA) scripts.

In the processing pipeline, cells were classified into three putative cell types: narrow interneurons, wide interneurons, and pyramidal cells. Interneurons were selected by 2 separate criteria; narrow interneurons were assigned if the waveform trough-to-peak latency was less than 0.425 ms. Wide interneuron was assigned if the waveform trough-to-peak latency was more than 0.425 ms and the rise time of the autocorrelation histogram was more than 6 ms. The remaining cells were assigned as pyramidal cells⁷⁸. We have isolated 1438 putative single units from 7 animals in 20 sessions ($n = 1150$ putative pyramidal cells, $n = 288$ putative interneurons) during the ThermoMaze behavior. We also collected 228 putative pyramidal cells from 2 animals in 3 control sessions (Suppl. Fig. 5) and 434 putative single units from 4 mice in 7 sessions using the 20-minute warmth paradigm (Fig. 6).

Pyramidal cells firing rate maps and SPW-R rate maps

To visualize and compare the spatial tuning properties of neurons across sub-sessions (Pre, Cooling and Post) during movement (speed ≥ 2.5 cm/s), we first binned the ThermoMaze ROI into 25 by 25 bins (each with size 1 x 1 cm) and counted the number of spikes of a neuron that occurred in each bin when the animal was actively moving (“movement spike-count map”). Next, we summed the total duration of time (in seconds) that the animal spent moving in each spatial bin to construct the “movement occupancy map”. The sub-session rate map of a cell during movement was computed by dividing the spike-count map by the occupancy map bin-wise. Similarly, we computed the SPW-R rate map within a sub-session by dividing the number of ripples that occurred in each bin by the total duration of immobility (speed < 2.5 cm/s) that the animal spent in each bin. Both firing rate maps and SPW-R rate maps were spatially smoothed using a 2-bin smoothing window (https://github.com/buzsakilab/buzcode/blob/6418ba3b4307c673988bcf6ca44b15927fef5a7d/externalPackages/FMAToolbox/Analyses/bz_Map.m).

Spatial tuning of spikes during SPW-Rs

To quantify the spatial tuning of neurons during SPW-Rs (Figure 5), we defined a metric called “within-ripple spatial tuning score” which is a value between 0 and 1. The higher score indicates stronger spatial tuning of a neuron during SPW-Rs. We first binned the ThermoMaze ROI into four quadrants (2x2) and determined the firing rate of the neuron in each quadrant

within SPW-Rs (i.e., total number of spikes of the cell divided by the total duration of SPW-R in that quadrant). For each SPW-R, a 300 ms time window surrounding the ripple's power peak time was taken and the temporal overlaps between SPW-Rs were removed. Next, the within-SPW-R firing rate ratio in a given quadrant (e.g., in quadrant A), is defined to be the firing rate of the neuron during SPW-Rs in quadrant A divided by the sum of the within-SPW-R firing rate in all four quadrants. Finally, the within-ripple spatial tuning score (Figure 5) of a neuron is defined to be the maximum within-SPW-R firing rate ratio of the cell among all quadrants. To test the hypothesis that such spatial tuning exists beyond chance level, we generated shuffled within-SPW-R firing rate maps by randomly assigning one of the four quadrants to each SPW-R. Specifically, we randomly permuted the location of the SPW-Rs so that the number of SPW-Rs per quadrant was kept fixed for the shuffled condition.

Bayesian decoding of the animal position

Bayesian decoding of the animal's position was based on the method provided by Zhang et al., 1998)⁴². In short, we utilized the spatial firing rate maps constructed to find the location that maximally explains the observation of spiking within a certain time window. Because SPW-Rs occurred mainly in the corners where the warm spots were, we simplified the analysis and binned the ThermoMaze into 2x2 quadrants, which yielded four maze areas. We constructed the firing rate map templates $f_i(x)$ of each neuron during SPW-Rs (300 ms time window surrounding the peak of each SPW-Rs) within the Cooling sub-session. The decoded position was then determined to be the quadrant that maximizes the posterior likelihood given the observed spike counts:

$$P(x | \mathbf{n}) = C(\tau, \mathbf{n}) P(x) \left(\prod_{i=1}^N f_i(x)^{n_i} \right) \exp \left(-r \sum_{i=1}^N f_i(x) \right)$$

where x was the quadrant index, \mathbf{n} was the spike counts vector observed surrounding the frame time, τ was the time window size and equals 300 ms, $C(\tau, \mathbf{n})$ was a normalization factor and was taken to be 1, $P(x)$ was the prior probability distribution of animal location and was taken to be 1 in the case of Figure 5D, i was the index of each cell, $f_i(x)$ was the average firing rate of cell i at position x , and N was the total number of pyramidal cells recorded in the session. For the purpose of cross-validation, we divided the SPW-Rs in each session into 100 folds. For each fold (testing dataset), the firing rate map templates were constructed using SPW-Rs from the other 99 folds (training dataset), and the decoding accuracy for the omitted fold was computed as the proportion of SPW-Rs whose corresponding quadrant was correctly decoded over the total number of SPW-Rs in the fold. For each session, we report the average decoding accuracy of test datasets.

Comparison of spatial tuning during SPW-Rs and movement

To quantify the similarity between spatial tuning of neurons during SPW-R and movement (theta oscillation), we calculated the firing rate ratios during movement in a similar way as we calculated the within-SPW-R firing rate ratios (see section "Spatial tuning during SPW-Rs" above). The ThermoMaze ROI was again binned into quadrants and firing rate maps (2x2) of each neuron during movement were calculated. The firing rate ratio of a neuron in each quadrant during movement was defined as the quadrant with the actual firing rate in that

quadrant divided by its mean firing rate in all quadrants. Next, the Pearson correlation between the firing rate ratios during SPW-Rs and movement in each quadrant for each cell within the Cooling sub-sessions were calculated.

We also studied the correlation between pyramidal cells' spatial tuning during SPW-Rs and movement at a population level (Fig. 6G). In each session, we first constructed population vectors in each quadrant by concatenating the firing rate ratio of each cell in a quadrant into a vector during SPW-R or movement. We then computed the pairwise correlation coefficients among the four population vectors between each condition in the correlation matrix and took the average across sessions.

Place cells identification

Data recorded in the ThermoMaze was used for analyzing the spatial tuning of spiking activity. Each session was split into three sub-sessions and all the criteria described below were independently applied to each sub-session. Putative pyramidal units with peak firing rates lower than 0.4 Hz and spatial information content^{80,81} lower than 0.25 bits/spike were not considered place cells⁸². We further computed the chance-level spatial information distribution by generating 100 shuffle datasets (by parsing spike trains and the mouse position during running into 5-s blocks and randomly shuffling the temporal correspondence between the spiking and position bins). If the z-scored spatial information (according to the chance-level spatial information distribution) is smaller than 1.65 (P-value > 0.05 in a one-sided test), the cell was not considered to be a place cell^{82,83}. In the end, a pyramidal neuron is determined to be a place cell throughout the entire session if it meets the criteria in all three individual sub-sessions.

REFERENCES

1. Buzsáki, G., and Tingley, D. (2023). Cognition from the Body-Brain Partnership: Exaptation of Memory. *Annu. Rev. Neurosci.* 46, 191–210. 10.1146/annurev-neuro-101222-110632.
2. Greaves, J.H., and Barnett, S.A. (1977). The Rat: A Study in Behavior. *J. Appl. Ecol.* 14, 649. 10.2307/2402575.
3. Vanderwolf, C.H. (1969). Hippocampal electrical activity and voluntary movement in the rat. *Electroencephalogr. Clin. Neurophysiol.* 26, 407–418. 10.1053/j.semss.2007.06.005.
4. Buzsáki, G., Bickford, R.G., Ponomareff, G., Thal, L.J., Mandel, R., and Gage, F.H. (1988). Nucleus basalis and thalamic control of neocortical activity in the freely moving rat. *J. Neurosci.* 8, 4007–4026. 10.1523/jneurosci.08-11-04007.1988.
5. Devilbiss, D.M., and Waterhouse, B.D. (2004). The effects of tonic locus ceruleus output on sensory-evoked responses of ventral posterior medial thalamic and barrel field cortical neurons in the awake rat. *J. Neurosci.* 24, 10773–10785. 10.1523/JNEUROSCI.1573-04.2004.
6. Dringenberg, H.C., and Vanderwolf, C.H. (1997). Neocortical activation: Modulation by multiple pathways acting on central cholinergic and serotonergic systems. *Exp. Brain Res.* 116, 160–174. 10.1007/PL00005736.
7. Harris, K.D., and Thiele, A. (2011). Cortical state and attention. *Nat. Rev. Neurosci.* 12, 509–523. 10.1038/nrn3084.
8. Methner, R., Cox, C.L., and Ashe, J.H. (1992). Cellular bases of neocortical activation: Modulation of neural oscillations by the nucleus basalis and endogenous acetylcholine. *J. Neurosci.* 12, 4701–4711. 10.1523/jneurosci.12-12-04701.1992.
9. McCormick, D.A., Nestvogel, D.B., and He, B.J. (2020). Neuromodulation of Brain State and Behavior. *Annu. Rev. Neurosci.* 43, 391–415. 10.1146/annurev-neuro-100219-105424.
10. Buzsáki, G., Leung, L.W., and Vanderwolf, C.H. (1983). Cellular bases of hippocampal EEG in the behaving rat. *Brain Res.* 287, 139–171. 10.1016/0165-

- 0173(83)90037-1.
11. Carandini, M., and Churchland, A.K. (2013). Probing perceptual decisions in rodents. *Nat. Neurosci.* *16*, 824–831. 10.1038/nn.3410.
12. Pisula, W., and Siegel, J. (2005). Exploratory behavior as a function of environmental novelty and complexity in male and female rats. *Psychol. Rep.* *97*, 631–638. 10.2466/pr0.97.2.631-638.
13. Ormond, J., and O’Keefe, J. (2022). Hippocampal place cells have goal-oriented vector fields during navigation. *Nature* *607*, 741–746. 10.1038/s41586-022-04913-9.
14. Kay, K., and Frank, L.M. (2019). Three brain states in the hippocampus and cortex. *Hippocampus* *29*, 184–238. 10.1002/hipo.22956.
15. Wilson, M.A., and McNaughton, B. (1994). Reactivation of Hippocampal Ensemble Memories During Sleep. *Science* (80-.). *265*, 676–679.
16. Allen, W.E., Chen, M.Z., Pichamoorthy, N., Tien, R.H., Pachitariu, M., Luo, L., and Deisseroth, K. (2019). Thirst regulates motivated behavior through modulation of brainwide neural population dynamics. *Science* (80-.). *364*, 0–10. 10.1126/science.aav3932.
17. Toth, L.A., and Gardiner, T.W. (2000). Food and Water Restriction Protocols: Physiological and Behavioral Considerations. *Contemp. Top. Lab. Anim. Sci.* *39*, 9–17.
18. Hughes, J.E., Amyx, H., Howard, J.L., Nanry, K.P., and Pollard, G.T. (1994). Health effects of water restriction to motivate lever-pressing in rats. *Lab. Anim. Sci.* *44*, 135–140.
19. Collier, G., and Levitsky, D. (1967). Defense of Water Balance in Rats: Behavioral and Physiological Responses To Depletion. *J. Comp. Physiol. Psychol.* *64*, 59–67. 10.1037/h0024800.
20. Malvache, A., Reichinnek, S., Villette, V., Haimerl, C., and Cossart, R. (2016). Awake hippocampal reactivations project onto orthogonal neuronal assemblies. *Science* (80-.). *353*, 1280–1283. 10.1126/science.aaf3319.
21. Foster, D.J., and Wilson, M.A. (2006). Reverse replay of behavioural sequences in hippocampal place cells during the awake state. *Nature* *440*, 680–683. 10.1038/nature04587.
22. Kay, K., Sosa, M., Chung, J.E., Karlsson, M.P., Larkin, M.C., and Frank, L.M. (2016). A hippocampal network for spatial coding during immobility and sleep. *Nature* *531*, 185–190. 10.1038/nature17144.
23. McEwen, B.S., Eiland, L., Hunter, R.G., and Miller, M.M. (2012). Stress and anxiety: Structural plasticity and epigenetic regulation as a consequence of stress. *Neuropharmacology* *62*, 3–12. 10.1016/j.neuropharm.2011.07.014.
24. Foster, T.C., Castro, C.A., and McNaughton, B.L. (1989). Spatial selectivity of rat hippocampal neurons: Dependence on preparedness for movement. *Science* (80-.). *244*, 1580–1582. 10.1126/science.2740902.
25. Garber, J.C., Barbee, R.W., Bielitzki, J.T., Clayton, L.A., Donovan, J.C., Hendriksen, C.F.M., Kohn, D.F., Lipman, N.S., Locke, P.A., Melcher, J., et al. (1996). Guide for the care and use of laboratory animals Eighth. (The National Academic Press).

- 749 26. Skop, V., Guo, J., Liu, N., Xiao, C., Hall, K.D., Gavrilova, O., and Reitman, M.L.
750 (2020). Mouse Thermoregulation: Introducing the Concept of the Thermoneutral
751 Point. *Cell Rep.* 31, 139–148. 10.1053/j.gastro.2016.08.014.CagY.
- 752 27. Maloney, S.K., Fuller, A., Mitchell, D., Gordon, C., and Michael Overton, J. (2014).
753 Translating animal model research: Does it matter that our rodents are cold?
754 *Physiology* 29, 413–420. 10.1152/physiol.00029.2014.
- 755 28. Gordon, C.J. (1993). *Temperature Regulation in Laboratory Rodents* (Cambridge
756 University Press) 10.1017/cbo9780511565595.
- 757 29. Gaskill, B.N., Rohr, S.A., Pajor, E.A., Lucas, J.R., and Garner, J.P. (2009). Some like
758 it hot: Mouse temperature preferences in laboratory housing. *Appl. Anim. Behav. Sci.*
759 116, 279–285. 10.1016/j.applanim.2008.10.002.
- 760 30. Kanosue, K., Hosono, T., Zhang, Y.H., and Chen, X.M. (1998). Neuronal networks
761 controlling thermoregulatory effectors. *Prog. Brain Res.* 115, 49–62. 10.1016/s0079-
762 6123(08)62029-4.
- 763 31. Gaskill, B.N., Rohr, S.A., Pajor, E.A., Lucas, J.R., and Garner, J.P. (2011). Working
764 with what you’ve got: Changes in thermal preference and behavior in mice with or
765 without nesting material. *J. Therm. Biol.* 36, 193–199. 10.1016/j.jtherbio.2011.02.004.
- 766 32. Gordon, C.J., Becker, P., and Ali, J.S. (1998). Behavioral thermoregulatory responses
767 of single- and group-housed mice. *Physiol. Behav.* 65, 255–262. 10.1016/S0031-
768 9384(98)00148-6.
- 769 33. Chen, X.M., Hosono, T., Mizuno, A., Yoda, T., Yoshida, K., Aoyagi, Y., and
770 Kanosue, K. (1998). New apparatus for studying behavioral thermoregulation in rats.
771 *Physiol. Behav.* 64, 419–424. 10.1016/S0031-9384(98)00094-8.
- 772 34. FLIR (2016). *Infrared Camera Accuracy and Uncertainty in Plain Language*. 1–4.
- 773 35. Muller, R.U., and Kubie, J.L. (1987). The effects of changes in the environment on the
774 spatial firing of hippocampal complex-spike cells. *J. Neurosci.* 7, 1951–1968.
775 10.1523/jneurosci.07-07-01951.1987.
- 776 36. Petersen, P.C., Voroslakos, M., and Buzsáki, G. (2022). Brain temperature affects
777 quantitative features of hippocampal sharp wave ripples. *J. Neurophysiol.* 127, 1417–
778 1425. 10.1152/jn.00047.2022.
- 779 37. Moser, E., Mathiesen, I., and Andersen, P. (1993). Association between brain
780 temperature and dentate field potentials in exploring and swimming rats. *Science* (80-
781). 259, 1324–1326. 10.1126/science.8446900.
- 782 38. Kiyatkin, E.A. (2010). Brain temperature homeostasis: Physiological fluctuations and
783 pathological shifts. *Front. Biosci.* 15, 73–92. 10.2741/3608.
- 784 39. Gordon, C.J. (1985). Relationship between autonomic and behavioral thermoregulation
785 in the golden hamster. *Physiol. Behav.* 34, 687–690. 10.1152/ajpregu.1986.251.2.r320.
- 786 40. Morris, R. (1984). Developments of a water-maze procedure for studying spatial
787 learning in the rat. *J. Neurosci. Methods* 11, 47–60. 10.1016/0165-0270(84)90007-4.
- 788 41. Leutgeb, S., Leutgeb, J.K., Barnes, C.A., Moser, E.I., McNaughton, B.L., and Moser,
789 M.B. (2005). Neuroscience: Independent codes for spatial and episodic memory in
790 hippocampal neuronal ensembles. *Science* (80-). 309, 619–623.
791 10.1126/science.1114037.

- 792 42. Zhang, K., Ginzburg, I., McNaughton, B.L., and Sejnowski, T.J. (1998). Interpreting
793 neuronal population activity by reconstruction: Unified framework with application to
794 hippocampal place cells. *J. Neurophysiol.* 79, 1017–1044. 10.1152/jn.1998.79.2.1017.
- 795 43. O’Keefe, J., and Nadel, L. (1978). *The Hippocampus as a Cognitive Map* (Oxford
796 University Press) 10.5840/philstudies19802725.
- 797 44. O’Neill, J., Senior, T., and Csicsvari, J. (2006). Place-selective firing of CA1
798 pyramidal cells during sharp wave/ripple network patterns in exploratory behavior.
799 *Neuron* 49, 143–155. 10.1016/j.neuron.2005.10.037.
- 800 45. Watson, B.O., Levenstein, D., Greene, J.P., Gelinas, J.N., and Buzsáki, G. (2016).
801 Network Homeostasis and State Dynamics of Neocortical Sleep. *Neuron* 90, 839–852.
802 10.1016/j.neuron.2016.03.036.
- 803 46. Breland, K., and Breland, M. (1961). The misbehavior of organisms. *Am. Psychol.* 16,
804 681–684. 10.1037/h0040090.
- 805 47. Buzsáki, G. (1982). The “Where is it?” reflex: Autoshaping the orienting response. *J.*
806 *Exp. Anal. Behav.* 37, 461–484.
- 807 48. Seligman, M.E. (1970). On the generality of the laws of learning. *Psychol. Rev.* 70,
808 406–418. 10.1037/h0069842.
- 809 49. Boakes, R.A., Poli, M., Lockwood, M.J., and Goodall, G. (1978). A study of
810 misbehavior: Token reinforcement in the rat. *J. Exp. Anal. Behav.* 29, 115–134.
- 811 50. Green, L., Tingley, D., Rinzel, J., and Buzsáki, G. (2022). Action-driven remapping of
812 hippocampal neuronal populations in jumping rats. *Proc. Natl. Acad. Sci. U. S. A.* 119.
813 10.1073/pnas.2122141119.
- 814 51. Krakauer, J.W., Ghazanfar, A.A., Gomez-Marin, A., MacIver, M.A., and Poeppel, D.
815 (2017). Neuroscience Needs Behavior: Correcting a Reductionist Bias. *Neuron* 93,
816 480–490. 10.1016/j.neuron.2016.12.041.
- 817 52. Brette, R. (2019). Is coding a relevant metaphor for the brain? *Behav. Brain Sci.*
818 10.1017/S0140525X19000049.
- 819 53. Cisek, P. (2019). A sensorimotor alternative to coding is possible. *Behav. Brain Sci.*
820 42, e222. 10.1017/S0140525X19001468.
- 821 54. Morrison, S.F., and Nakamura, K. (2019). Central Mechanisms for Thermoregulation.
822 *Annu. Rev. Physiol.* 81, 285–308. 10.1146/annurev-physiol-020518-114546.
- 823 55. Tansey, E.A., and Johnson, C.D. (2015). Recent advances in thermoregulation. *Adv.*
824 *Physiol. Educ.* 39, 139–148. 10.1152/advan.00126.2014.
- 825 56. Vallerand, A.L., Perusse, F., and Bukowiecki, L.J. (1987). Cold exposure potentiates
826 the effect of insulin on in vivo glucose uptake. *Am. J. Physiol. - Endocrinol. Metab.*
827 253. 10.1152/ajpendo.1987.253.2.e179.
- 828 57. Maickel, R.P., Matussek, N., Stern, D.N., and Brodie, B.B. (1967). The sympathetic
829 nervous system as a homeostatic mechanism. I. Absolute need for sympathetic nervous
830 function in body temperature maintenance of cold-exposed rats. *J. Pharmacol. Exp.*
831 *Ther.* 157.
- 832 58. Harding, E.C., Yu, X., Miao, A., Andrews, N., Ma, Y., Ye, Z., Lignos, L., Miracca, G.,
833 Ba, W., Yustos, R., et al. (2018). A Neuronal Hub Binding Sleep Initiation and Body
834 Cooling in Response to a Warm External Stimulus. *Curr. Biol.* 28, 2263–2273.e4.

- 835 10.1016/j.cub.2018.05.054.
- 836 59. Song, K., Wang, H., Kamm, G.B., Pohle, J., De Castro Reis, F., Heppenstall, P.,
837 Wende, H., and Siemens, J. (2016). The TRPM2 channel is a hypothalamic heat sensor
838 that limits fever and can drive hypothermia. *Science* (80-.). 353, 1393–1398.
839 10.1126/science.aaf7537.
- 840 60. Sterling, P., and Eyer, J. (1988). Allostasis: A new paradigm to explain arousal
841 pathology. In *Handbook of Life Stress, Cognition and Health*, S. Fisher and J. Reason,
842 eds. (John Wiley & Sons, Ltd).
- 843 61. Sterling, P. (2004). Principles of allostasis: Optimal design, predictive regulation,
844 pathophysiology, and rational therapeutics. *Allostasis, Homeostasis, Costs Physiol.*
845 *Adapt.*, 17–64. 10.1017/CBO9781316257081.004.
- 846 62. Schulkin, J., and Sterling, P. (2019). Allostasis: A Brain-Centered, Predictive Mode of
847 Physiological Regulation. *Trends Neurosci.* 42, 740–752. 10.1016/j.tins.2019.07.010.
- 848 63. Tan, C.L., and Knight, Z.A. (2018). Regulation of Body Temperature by the Nervous
849 System. *Neuron* 98, 31–48. 10.1016/j.neuron.2018.02.022.
- 850 64. Steimer, T. (2011). Animal models of anxiety disorders in rats and mice: Some
851 conceptual issues. *Dialogues Clin. Neurosci.* 13, 495–506.
852 10.31887/dens.2011.13.4/tsteimer.
- 853 65. Diba, K., and Buzsáki, G. (2007). Forward and reverse hippocampal place-cell
854 sequences during ripples. *Nat. Neurosci.* 10, 1241–1242. 10.1038/nn1961.
- 855 66. Dupret, D., O'Neill, J., Pleydell-Bouverie, B., and Csicsvari, J. (2010). The
856 reorganization and reactivation of hippocampal maps predict spatial memory
857 performance. *Nat. Neurosci.* 13, 995–1002. 10.1038/nn.2599.
- 858 67. Silva, D., Feng, T., and Foster, D.J. (2015). Trajectory events across hippocampal
859 place cells require previous experience. *Nat. Neurosci.* 18, 1772–1779.
860 10.1038/nn.4151.
- 861 68. Pfeiffer, B.E., and Foster, D.J. (2013). Hippocampal place-cell sequences depict future
862 paths to remembered goals. *Nature* 497, 74–79. 10.1038/nature12112.
- 863 69. Davidson, T.J., Kloosterman, F., and Wilson, M.A. (2009). Hippocampal Replay of
864 Extended Experience. *Neuron* 63, 497–507. 10.1016/j.neuron.2009.07.027.
- 865 70. Gupta, A.S., van der Meer, M.A.A., Touretzky, D.S., and Redish, A.D. (2010).
866 Hippocampal Replay Is Not a Simple Function of Experience. *Neuron* 65, 695–705.
867 10.1016/j.neuron.2010.01.034.
- 868 71. Karlsson, M.P., and Frank, L.M. (2009). Awake replay of remote experiences in the
869 hippocampus. *Nat. Neurosci.* 12, 913–918. 10.1038/nn.2344.
- 870 72. Dragoi, G., and Tonegawa, S. (2011). Preplay of future place cell sequences by
871 hippocampal cellular assemblies. *Nature* 469, 397–401. 10.1038/nature09633.
- 872 73. Grosmark, A.D., and Buzsáki, G. (2016). Diversity in neural firing dynamics supports
873 both rigid and learned hippocampal sequences. *Science* (80-.). 351, 1440–1443.
874 10.1126/science.aad1935.
- 875 74. Jarosiewicz, B., and Skaggs, W.E. (2004). Level of arousal during the small irregular
876 activity state in the rat hippocampal EEG. *J. Neurophysiol.* 91, 2649–2657.
877 10.1152/jn.01082.2003.

75. Voroslakos, M., Miyawaki, H., Royer, S., Diba, K., Yoon, E., Petersen, P., and Buzsáki, G. (2021). 3D-printed Recoverable Microdrive and Base Plate System for Rodent Electrophysiology. *Bio-Protocol* 11. 10.21769/bioprotoc.4137.
76. Vöröslakos, M., Petersen, P.C., Vöröslakos, B., and Buzsáki, G. (2021). Metal microdrive and head cap system for silicon probe recovery in freely moving rodent. *Elife* 10, 1–21. 10.7554/eLife.65859.
77. Mathis, A., Mamidanna, P., Cury, K.M., Abe, T., Murthy, V.N., Mathis, M.W., and Bethge, M. (2018). DeepLabCut: markerless pose estimation of user-defined body parts with deep learning. *Nat. Neurosci.* 21, 1281–1289. 10.1038/s41593-018-0209-y.
78. Petersen, P.C., Siegle, J.H., Steinmetz, N.A., Mahallati, S., and Buzsáki, G. (2021). CellExplorer: A framework for visualizing and characterizing single neurons. *Neuron* 109, 3594–3608.e2. 10.1016/j.neuron.2021.09.002.
79. Pachitariu, M., Steinmetz, N., Kadir, S., Carandini, M., and Harris, K.D. (2016). Kilosort: realtime spike-sorting for extracellular electrophysiology with hundreds of channels. *bioRxiv*, 061481.
80. Mizuseki, K., Royer, S., Diba, K., and Buzsáki, G. (2012). Activity dynamics and behavioral correlates of CA3 and CA1 hippocampal pyramidal neurons. *Hippocampus* 22, 1659–1680. 10.1002/hipo.22002.
81. Skaggs, W., McNaughton, B., and Gothard, K. (1992). An Information-Theoretic Approach to Deciphering the Hippocampal Code. In *Advances in Neural Information Processing Systems*, S. Hanson, J. Cowan, and C. Giles, eds. (Morgan-Kaufmann).
82. Roux, L., Hu, B., Eichler, R., Stark, E., and Buzsáki, G. (2017). Sharp wave ripples during learning stabilize the hippocampal spatial map. *Nat. Neurosci.* 20, 845–853. 10.1038/nn.4543.
83. Markus, E.J., Barnes, C.A., McNaughton, B.L., Gladden, V.L., and Skaggs, W.E. (1994). Spatial information content and reliability of hippocampal CA1 neurons: Effects of visual input. *Hippocampus* 4, 410–421. 10.1002/hipo.450040404.